This article has been accepted for publication in IEEE Journal of Selected Topics in Quantum Electronics. This is the author's version which has not been fully edited and content may change prior to final publication. Citation information: DOI 10.1109/JSTQE.2022.3185169

*

Mid-infrared supercontinuum generation in a varying dispersion waveguide for multi-species gas spectroscopy

Alberto Della Torre, Rémi Armand, Milan Sinobad, Kokou Firmin Fiaboe, Barry Luther-Davies, Stephen Madden, Arnan Mitchell, Thach Nguyen, David J. Moss, Jean-Michel Hartmann, Vincent Reboud, Jean-Marc Fedeli, Christelle Monat, and Christian Grillet

***Abstract*—We report the experimental generation of a broadband and flat mid-infrared supercontinuum in a silicon-germanium-on-silicon two-stage waveguide. Our particular design combines a short and narrow waveguide section for efficient supercontinuum generation, and an inverse tapered section that promotes the generation of two spectrally shifted dispersive waves along the propagation direction, leading to an overall broader and flatter supercontinuum. The experimentally generated supercontinuum extended from 2.4 to 5.5 µm, only limited by the long wavelength detection limit of our spectrum analyzer. Numerical simulations predict that the supercontinuum actually extends to 7.8 µm. We exploit the enhanced flatness of our supercontinuum for a proof-of-principle demonstration of free-space multi-species gas spectroscopy of water vapor and carbon dioxide.**

***Index Terms*—Mid-infrared, nonlinear optics, supercontinuum, spectroscopy**

I. INTRODUCTION

TRACE-GAS sensing is a rapidly growing field. Applications of gas-sensing systems can be found in the control of industrial processes for the detection of hazardous gases [1], [2], in environmental monitoring for the measurements of pollutants in air [1], [3], in health care for the diagnosis of diseases [4] and in food quality control [5]. Thanks to the strong absorption fingerprint of many important molecules, the mid-infrared (MIR, and the 3-13 µm band in particular) spectral region is particularly attractive for spectroscopic and sensing applications [6]. Despite its potential, commercial MIR technology is, for the moment, limited to bulky and expensive stand-alone devices. The integration of MIR photonic systems onto a group IV platform would enable us to leverage standard microfabrication technologies for the large-scale production of compact and cost-effective sensing devices. The last few years have witnessed a remarkable growth of research activity in integrated group IV MIR photonics [7]–[10], which is starting to become a mature technology.

Integrated light sources are an important element of compact spectroscopic devices. In the MIR, the dominant technologies are quantum cascade lasers and interband cascade lasers [11], [12]. However, they are not widely tunable in wavelength, and an array of different lasers must be used to cover a wide spectral range [13]. In addition, the number of emission lines is limited by the number of multiplexed lasers. In comparison, supercontinuum (SC) sources can cover a spectral band of more than one octave. SC sources are,

*This work was supported by the Agence Nationale de la Recherche (ANR) (Grant No. MIRSiCOMB, ANR-17-CE24-0028), the H2020 European Research Council (ERC) (Grant No. GRAPHICS, 648546), the Horizon 2020 research and innovation programme under the Marie Skłodowska-Curie Actions (MSCA) (ECLAUSion, grant agreement No 801512). We acknowledge Lynred® for lending us the mid-infrared camera and the support of the International Associated Laboratory in Photonics between France and Australia (LIA ALPhFA).

Corresponding author: A. Della Torre

Alberto Della Torre is with the Université de Lyon, Institut des Nanotechnologies de Lyon, UMR CNRS 5270, Ecully, France (e-mail: alberto.della-torre@ ec-lyon.fr).

Remi Armand is with the Université de Lyon, Institut des Nanotechnologies de Lyon, UMR CNRS 5270, Ecully, France (e-mail: remi.armand@ ec-lyon.fr).

Milan Sinobad is with the Deutsches Elektronen-Synchrotron, 22607 Hamburg, Germany (e-mail: milan.sinobad@desy.de).

Kokou Firmin Fiaboe is with the Université de Lyon, Institut des Nanotechnologies de Lyon, UMR CNRS 5270, Ecully, France, and with the RMIT University, School of Engineering Melbourne, VIC 3001, Australia (e-mail: kokou-firmin.fiaboe@ec-lyon.fr).

Barry Luther-Davies is with The Australian National University, Quantum Science and Technology, Canberra, ACT 2600, Australia (e-mail: barry.luther-davies@anu.edu.au).

Stephen Madden is with The Australian National University, Quantum Science and Technology, Canberra, ACT 2600, Australia (e-mail: stephen.madden@anu.edu.au).

Arnan Mitchell is with the RMIT University, School of Engineering Melbourne, VIC 3001, Australia (e-mail: arnan.mitchell@rmit.edu.au).

Thach Nguyen is with the RMIT University, School of Engineering Melbourne, VIC 3001, Australia (e-mail: thach.nguyen@rmit.edu.au).

Jean-Michel Hartmann is with the Université Grenoble Alpes, CEA-Leti, 38054 Grenoble Cedex 9, France (e-mail: jean-michel.hartmann@cea.fr).

Vincent Reboud is with the Université Grenoble Alpes, CEA-Leti, 38054 Grenoble Cedex 9, France (e-mail: vincent.reboud@cea.fr).

Jean-Marc Fedeli was with the Université Grenoble Alpes, CEA-Leti, 38054 Grenoble Cedex 9, France (e-mail: jean-marc.fedeli@cea.fr).

Christelle Monat is with the Université de Lyon, Institut des Nanotechnologies de Lyon, UMR CNRS 5270, Ecully, France (e-mail: christelle.monat@ ec-lyon.fr).

Christian Grillet is with the Université de Lyon, Institut des Nanotechnologies de Lyon, UMR CNRS 5270, Ecully, France (e-mail: christian.grillet@ ec-lyon.fr).

therefore, ideal for high-resolution multi-species molecular spectroscopy [14], [15].

In recent years, there have been a few demonstrations of MIR SC generation in group IV waveguides [16]–[24]. The properties of the generated SC strongly depend on the group velocity dispersion profile of the underlying waveguide. The SC bandwidth is maximal in waveguides pumped in the anomalous dispersion region, but the generated spectrum typically suffers from low flatness and poor coherence [25]. On the other hand, high spectral flatness and coherence can be achieved in all-normal dispersion (ANDi) waveguides with, however, a narrower spectral span [26]. Our team has demonstrated SC generation up to 8.5 µm in a straight silicon-germanium-on-silicon (SiGe/Si) waveguide operating in the anomalous dispersion regime [19], as well as a narrower, but flat and fully coherent SC in a ANDi SiGe/Si straight waveguide [22]. Multi-species absorption spectroscopy would greatly benefit from a SC that combines high spectral flatness and a broad spectral coverage, i.e. from a design that overcomes this tradeoff.

Shortly after the first demonstrations of SC generation in optical fibers, a number of experimental results showed that the flatness and bandwidth of the SC can be improved by varying the dispersion along the propagation direction. In 1997, J. W. Lou *et al.* used a fiber with decreasing dispersion and zero-dispersion wavelength (ZDW) varying from 1538 to 1549 nm to generate a broader and smoother spectrum than in a fiber with constant dispersion [27]. Several demonstrations of SC generation in tapered fibers have been reported in the following years [28]–[36]. Most often, the idea is to continuously shift the ZDW, which corresponds to a variation of the phase-matching condition for dispersive wave (DW) generation and Four-Wave Mixing, thereby enhancing the energy transfer to new wavelengths. Recently, advances in micro-fabrication technology have made it possible to leverage tapered designs in integrated platforms as well, and, potentially, with a higher degree of flexibility. The first experimental demonstration was achieved by Singh *et al.* in 2019 [37]. An octave spanning SC, extending from 1.2 to 2.4 µm, was generated in a horizontally tapered silicon-on-silica (SOI) rib waveguide buried in silica, in which the dispersion profile was varied by continuously changing the waveguide width along its length. Compared to straight waveguides of similar dimensions, the authors demonstrated a 400 nm broader SC in the tapered waveguide, as well as improved coherence thanks to the suppression of the modulation instability. Similar results have also been achieved in 2020 by Wei *et al.* in an air-clad SOI waveguide working in the near and short-wavelength infrared region [38].

In this work, we employed an air-clad SiGe/Si two-stage inverse-tapered waveguide to efficiently generate a MIR SC with enhanced spectral flatness and spectral coverage. A first short and narrow section was pumped at 3.9 µm in the anomalous dispersion regime for promoting efficient SC generation. Then, a second inverse-tapered section was employed to continuously shift the two ZDWs towards longer wavelengths. The experimentally generated SC extended from 2.4 to 5.5 µm, limited at the longer wavelengths by the detection limit of our spectrum analyzer. Numerical simulations predict a long wavelength SC extension up to 7.8 µm. As compared to straight waveguides, the particular design of our two stage dispersion varying waveguide improved the SC flatness, particularly in the 2.4-3 µm wavelength range, and increased its long-wavelength extension. We harnessed the enhanced quality of our SC for a proof-of-principle demonstration of multi-species gas spectroscopy. In particular, the improved SC flatness enables us to simultaneously measure the absorption spectrum of water and carbon dioxide at around 2.7 and 4.2 µm, respectively.

II. WAVEGUIDE DESIGN

Our main goal is to improve the flatness of the SC in the 2.5-3 µm and 4.2-4.3 µm spectral regions, which are of interest for the detection of water vapor and carbon dioxide. At the same time, we targeted a design that generates a broad SC with low input power. To maximize the efficiency of the SC generation process, it is preferable to employ a waveguide with a small cross-section, since a low modal effective area enhances the nonlinear transfer of energy towards new wavelengths [39]. However, this would not be the optimal design to maximize the SC bandwidth. Indeed, an air-clad waveguide with a small-cross section area typically has a cutoff wavelength which is much shorter than would be expected for one with a large-cross section, strongly limiting the SC extension at the long wavelength side. For instance, in ref. [19] we have shown that an air-clad SiGe/Si waveguide with a large cross-section (4.2 µm x 6 µm) could generate a SC extending beyond 8 µm, whereas a waveguide with a smaller cross-section (2.7 µm x 3.75 µm) introduced a cutoff at around 6 µm. Here, we employed an inverse-tapered waveguide to overcome this trade-off and efficiently generate a broadband SC which also exhibits high spectral flatness. A tapered waveguide with two increasing ZDWs can lead to increased spectral flatness at both the short and long wavelengths sides, thanks to the continuous variation of the phase-matching condition for the generation of DWs. The continuous spectral shift of the blue DW fills the gap that is often present between the DW and the rest of the SC, whereas the shift of the red DW increases the SC extension to longer wavelengths. The final design thus consists of a two stage waveguide: a 3 mm long straight input section exhibits a small cross-section for efficient SC generation, whereas a second part with an increasingly larger cross-section extends the cutoff, and therefore the maximal SC extension, to longer wavelengths. The length of the first straight section was chosen so that the DWs would start being generated in the smaller cross-section part, to achieve most of the spectral broadening at the beginning of the waveguide. This should result in a flatter and slightly broader output spectrum.

More specifically, the whole design consisted of a 2.3 cm long, 3.3 µm thick $Si_{0.6}Ge_{0.4}$/Si waveguide with varying width along its length (fig. 1a). The waveguide was designed to be pumped at 3.9 µm wavelength with TE polarization. The input side starts with a 3 mm long, 3.25 µm wide straight section, which has an anomalous dispersion region between 3.5 and 4.9 µm (fig. 1b, blue curve). This first section has a cutoff wavelength around 5.2 µm, and is single-mode at the pump wavelength. The waveguide width was then linearly increased up to 9 µm at the output. In this tapered section, the waveguide is multi-mode for widths higher than 4 µm. During the

This article has been accepted for publication in IEEE Journal of Selected Topics in Quantum Electronics. This is the author's version which has not been fully edited and content may change prior to final publication. Citation information: DOI 10.1109/JSTQE.2022.3185169

experimental measurements, we made sure that the coupling to higher-order modes was low by having a single Gaussian profile on the MIR camera at the waveguide output. The change in the waveguide width corresponded to a continuous change of its dispersion, and the two ZDWs shift towards longer wavelengths (fig. 1b). For a width of 6 µm, the two ZDW are at 4.67 and 6.1 µm (fig. 1b, purple curve). Above ~8 µm width, the waveguide has an ANDi profile (fig. 1b, green curve) and is around 5 mm long. Besides shifting the ZDWs, the increasing width of the waveguide also shifts the cutoff wavelength to beyond 9 µm.

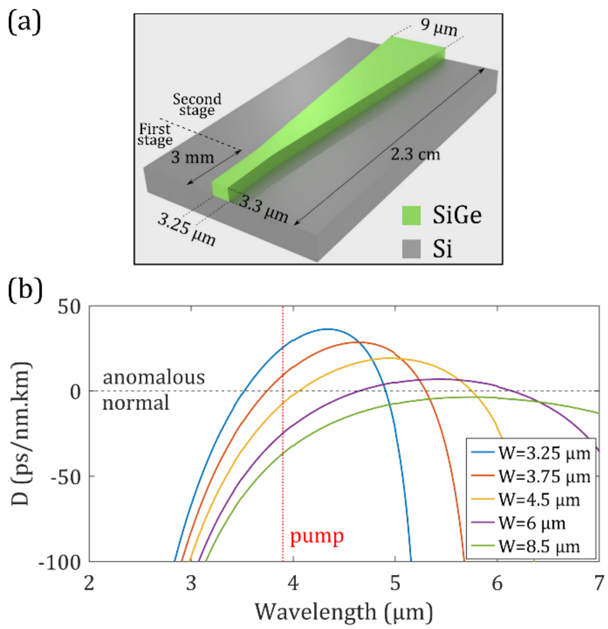

Fig. 1. (a) Schematic of the two-stage dispersion varying SiGe/Si waveguide. (b) Dispersion profile (calculated in Lumerical MODE) for selected waveguide widths.

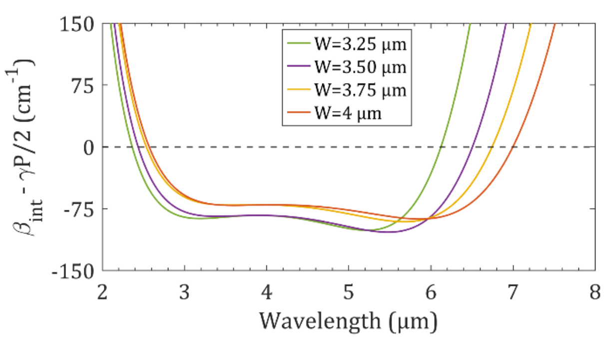

Fig. 2. (a) Calculated soliton-DW phase mismatch at 2.73 kW coupled peak power for straight waveguides of selected widths. The γ parameter is equal to 1, 0.94, 0.88 and 0.82 $(Wm)^{-1}$ for 3.25, 3.5, 3.75 and 4 µm wide waveguides, respectively. For waveguides wider than ~4 µm, the pump is in the normal dispersion regime and dispersive waves are not generated.

The shift of the ZDW implies a continuous variation of the phase-matching condition that sustains the generation of the DWs. The DWs are generated in the normal dispersion region by phase-matched transfer of energy from a soliton in the anomalous dispersion region. The phase mismatch Δk between the DW and the soliton is approximately given by [25]:

$$\Delta k = \beta(\omega) - \beta(\omega_s) - v_g^{-1}(\omega - \omega_s) - \frac{\gamma P}{2}$$

where β is the phase constant, ω_s is the frequency of the soliton, v_g is the group velocity, P is the pulse peak power and γ is the waveguide nonlinear parameter. The first three terms on the right are also called integrated dispersion β_{int}. The DWs will be generated at the spectral positions for which $\Delta k = \beta_{int} - \gamma P/2 = 0$. Fig. 2 shows the phase mismatch for four selected waveguide widths considering a coupled peak power of 2.73 kW. These were calculated assuming a soliton frequency equal to the pump frequency. For each waveguide width, DWs are expected to be generated where the phase mismatch is zero. As expected, the change in the ZDWs due to the waveguide width variation results in an increase of the wavelengths at which the DW should be generated, both on the short and long wavelength sides.

III. SUPERCONTINUUM GENERATION

We fabricated the two-stage dispersion varying waveguide and a set of straight waveguides with different widths by the same method as in ref. [19]. We performed linear and nonlinear measurements using a tunable Optical Parametric Amplifier (OPA, Hotlight Systems MIROPA-fs) delivering ≈200 fs pulses at 63 MHz repetition rate and with a tunable wavelength around 4 µm. We used a set of two polarizers and a half wave-plate to control the input power and polarization. Light was coupled to the waveguide and the output was collected with the help of two MIR lenses, a visible camera (Dino-lite) and a MIR camera (Lynred). The transmitted power was measured with a fast photodetector (Thorlabs PDAVJ10), and the generated SC spectrum was recorded using an Optical Spectrum Analyzer (OSA, Thorlabs OSA205) sensitive from <2 µm to 5.5 µm. We used a lock-in amplification scheme to reduce the impact of thermal noise. We measured the propagation loss in 3.25, 3.75 and 4 µm wide waveguides of constant width by probing spiral waveguides of different lengths under relatively low average powers (<1 mW), using the method described in ref. [24]. The resulting losses in the 3.25-4.1 µm wavelength range were lower than 1 dB/cm for these widths and were as low as 0.12 dB/cm at 3.9 µm for the 4 µm wide waveguide (fig. 3). Waveguides wider than 4 µm exhibited even lower losses (due to lower interaction of the mode field with the waveguide sidewalls). The length difference between the waveguides was then too low to extract reliable propagation losses in that case.

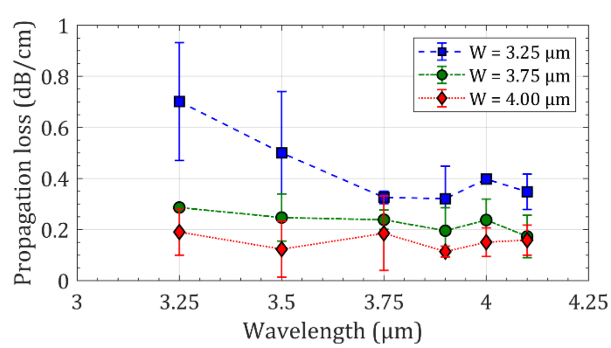

Fig. 3. Propagation loss of the fundamental TE mode at different wavelengths measured in straight 3.25 (blue squares), 3.75 (green circles), and 4 (red diamond) µm wide waveguides.

The SC spectra were generated by increasing the coupled peak (average) power up to 4.5 kW (30 mW). Fig. 4(a) shows a map of the experimental spectra. At high powers, the SC extends from ≈2.4 µm up to the detection limit of the OSA at 5.5 µm. Simulated spectra (fig. 4b) were calculated by numerically solving the generalized nonlinear Schrödinger equation (GNLSE), which describes the propagation of short optical pulses in the waveguide [25]. These extend well beyond the detection limit of the OSA, with a 1.6 octave spanning SC up to 7.8 µm at the maximum coupled peak power of 4.5 kW. The tapered waveguide section was modelled by solving the GNLSE in 256 ~90 µm long sections of constant widths (linearly increasing from 3.25 up to 9 µm) and using the calculated output from one section as the input for the following one. As a conservative estimate, the propagation losses were considered constant and equal to 0.3 dB/cm, i.e. the value at the pump wavelength for the input width (3.25 µm, fig. 3). We used the same nonlinear coefficients for the SiGe core material as in ref. [22], i.e. a Kerr index $n_2 = 4 \text{ x } 10^{-18}$ m^2/W and a four-photon absorption coefficient $\alpha_{4PA} = 1.16 \text{ x } 10^{-42}$ m^5/W^3, corresponding to γ=1 (Wm)$^{-1}$ and γ=0.37 (Wm)$^{-1}$ at the waveguide input and output, respectively. Like in ref. [22], three-photon absorption was not included, since it is negligible at the pump wavelength. By measuring the insertion loss (equal to 11 dB) and assuming, as a conservative estimate, the same coupling losses at the input and output facets (~5.3 dB/facet), we can infer an on-chip SC average power higher than 3.5 mW for coupled peak powers greater than 2.5 kW. In comparison, the on-chip SC power retrieved from integrating the power spectral density measured by the OSA is not higher than 2.3 mW. This tends to confirm that, at high input powers, the SC extends beyond the OSA detection limit. The difference between the SC power measured with the photodetector and the OSA is then due to the undetected signal beyond 5.5 µm in the latter case. The bandwidth of this SC is comparable to that reported in 2018 by our group in ref. [19], i.e. the generation of a SC extending from 3 to 8.3 µm in a large cross-section SiGe/Si waveguide , but it is here achieved for lower pump power and more compact waveguides. Indeed, those prior results were obtained with a coupled peak power of 3.54 kW [19]. Here, thanks to the smaller cross-section of the waveguide in its first part and the subsequent cutoff wavelength shift to beyond 9 µm, the coupled peak power necessary to reach the maximal spectral extension is reduced to ≈2 kW, i.e. more than 40% lower than in ref. [19]. The SC flatness is also improved, in particular at the extreme parts of the spectrum (of ≈10 dB), and the waveguide length is highly reduced from 7 to 2.3 cm. We are now going to analyze, with the help of numerical simulations, how the DWs dynamics is crucial for the generation of our broad and flat SC.

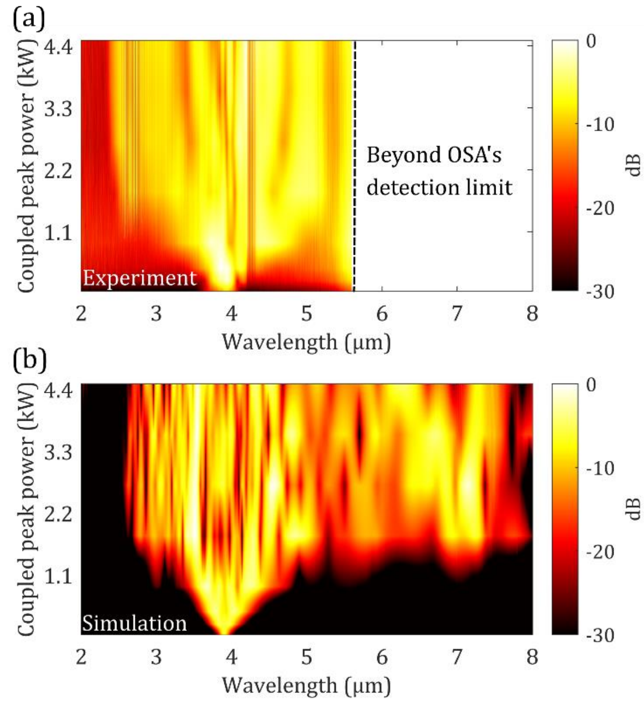

Fig. 4. Experimental (a) and simulated (b) SC generation in the two-stage dispersion varying waveguide for increasing coupled peak power. The high signal in fig. (a) beyond 5.3 µm even for low coupled peak powers is due to the increased noise floor of the OSA.

IV. DISCUSSION

Fig. 5 shows the experimental (a) and simulated (b) SCs generated at 2.73 kW coupled peak power in the 2.3 cm long two-stage dispersion varying waveguide, as well as in 2.2 cm long straight waveguides with different constant widths. The shaded areas indicate the spectral positions of the DWs as expected from the phase-matching condition for each waveguide width (fig. 2). First, we can notice that the position of the DWs is in relatively good agreement with the theory. The small difference with the theoretically predicted phase-matched wavelengths can be due to a slightly different central frequency of the soliton compared to the pump frequency used in the calculations. We can see how both the blue and red DWs shift towards longer wavelengths as the waveguide width increases (the red DW is visible only in the simulations, since it lies beyond the OSA detection limit). For waveguides wider than 4 μm, the pump wavelength is in the normal dispersion region (see fig. 1b). Dispersive waves are no longer generated then, and the SC bandwidth in the corresponding straight waveguides starts shrinking (see 4.25 μm wide waveguide), eventually reaching the flat and narrower spectra typical of SC generation in the ANDi regime (see the 8.5 μm wide waveguide). The continuous wavelength shift of the DWs results in the filling of the 2.4-3 µm and 6-7.8 µm spectral regions, leading to a flatter SC in the tapered than in the straight waveguide. In particular, the increased flatness at the blue end of the spectrum leads to better resolution of the dips around 2.7 µm that are due to the absorption from water vapor in the free-space path between the waveguide output and the OSA. Similar dips are also visible at around 4.2 μm due to the absorption from CO_2. Finally, the

This article has been accepted for publication in IEEE Journal of Selected Topics in Quantum Electronics. This is the author's version which has not been fully edited and content may change prior to final publication. Citation information: DOI 10.1109/JSTQE.2022.3185169

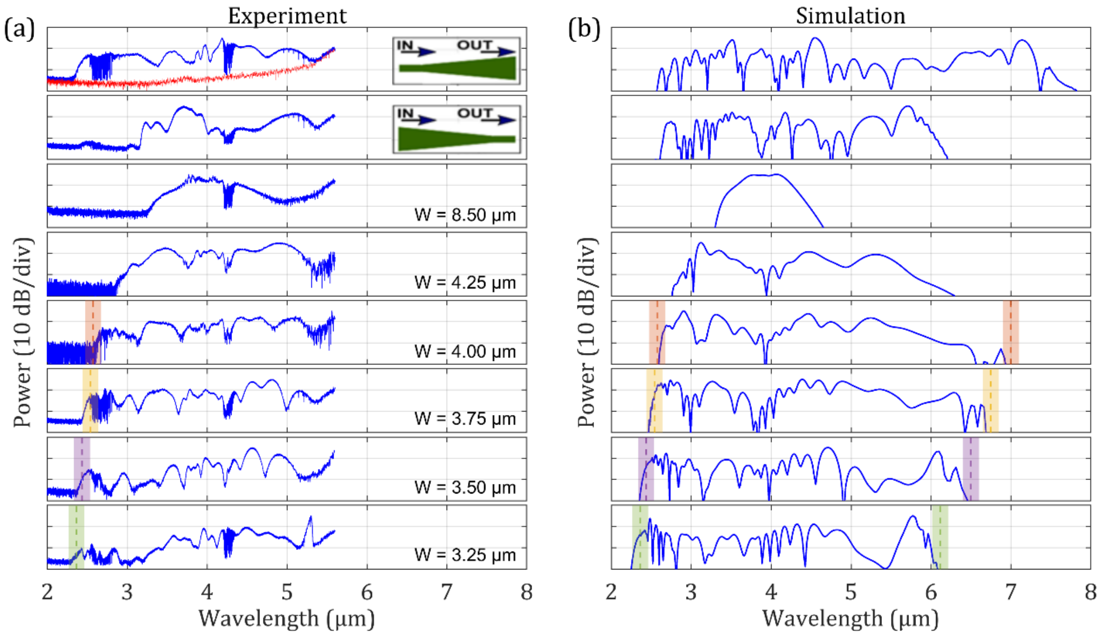

Fig. 5. Experimental (a) and simulated (b) SC generated at 2.73 kW coupled peak power in the two-stage dispersion varying waveguide (pumped from the narrow side, top, and from the wide side, second from top) and in waveguides of different constant widths. The shaded areas indicate 200 nm wide spectral regions around the wavelengths that satisfy the soliton-dispersive wave phase-matching condition (dashed lines). The rise of the experimental spectra at around 5.5 µm is due to the increased noise floor of the OSA (red spectrum in the top plot of fig. (a)).

second spectrum from the top in fig. 5 shows the SC measured when the waveguide is pumped from the wider side (i.e. the waveguide is rotated by 180°), to further emphasize the impact of our two-stage dispersion varying waveguide design on the SC properties. As expected, the spectrum is much narrower in this case, since dispersive waves are generated only towards the end of the waveguide, where the propagating pulse has already spread in time and the peak power is lowered. The lower signal below 3 μm in the experimental spectrum as compared to the simulation is due to water vapor absorption.

Fig. 6 shows the simulated spectral (a) and temporal (b) evolution along the waveguide length, calculated for 2.73 kW coupled peak power. Both the blue and red DWs shift towards longer wavelengths as the width of the waveguide gradually increases, filling the 2.4-3 and 6-7.8 µm spectral regions (blue and red shaded areas in the top plot of fig. 6a). After the initial shift of the ZDWs, the waveguide has, over the last 5 mm, an ANDi profile (see fig. 1b), which flattens the central part of the spectrum. In the time domain, we can clearly distinguish the signature of the blue (slower) and red (faster) DWs. We can also notice that dispersive waves start to be generated at the end of the first-stage 3 mm long narrow and straight section, indicated in fig. 6 by a white dashed line. This is in quite good agreement with the expected soliton fission length associated with the narrow entrance waveguide which, at this power, is around 5 mm. As typical in the SC generation in the anomalous dispersion regime, the soliton dynamics and dispersive waves generation results in a complex temporal profile at the waveguide output (fig. 6b, top). Different studies have shown numerically that the coherence of the SC is improved in tapered waveguides as compared to waveguides with constant width [37], [40]. This is due to the suppression of modulation instability in tapered waveguides, as a consequence of the continuous change of dispersion, and therefore of the maximum modulation instability gain frequency.

As a final remark, fig. 7 shows the calculated spectral evolution along a 2.3 cm long similarly tapered waveguide simulated without the first-stage straight section at the input at 2.73 kW coupled peak power. We can notice that, as compared to the two-stage waveguide of fig. 5a, (i) the spectrum is roughly 300 nm narrower at the short wavelength side (because dispersive waves are not yet generated in the initial part of the waveguide) and (ii) the overall spectral flatness is degraded. This highlights the added value of the first-stage straight section to improve the quality of the SC in terms of bandwidth and flatness.

This article has been accepted for publication in IEEE Journal of Selected Topics in Quantum Electronics. This is the author's version which has not been fully edited and content may change prior to final publication. Citation information: DOI 10.1109/JSTQE.2022.3185169

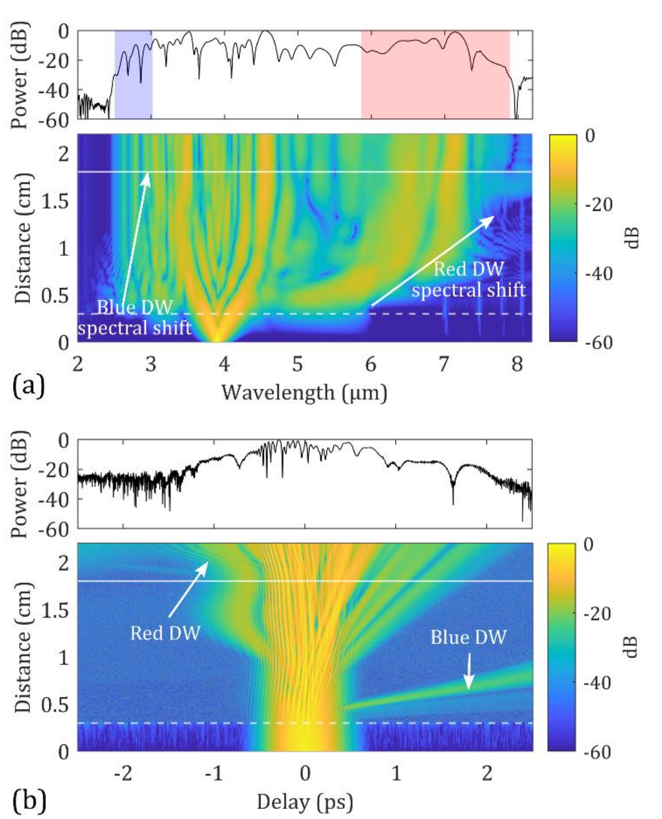

Fig. 6. (a) Bottom: spectral evolution at different distances along the two stage dispersion varying waveguide and corresponding wavelength shift of the dispersive waves. Top: Spectrum at the output of the waveguide. The shaded areas highlight the spectral regions filled by the DWs (at the -30 dB level). (b) Bottom: temporal evolution of the pulse at different distances along the waveguide. Top: temporal profile of the pulse at the output of the waveguide. Simulations were performed at 2.73 kW coupled peak power. The horizontal white dashed line indicates the boundary between the first (narrow straight section) and second stage (tapered section) of the waveguide.

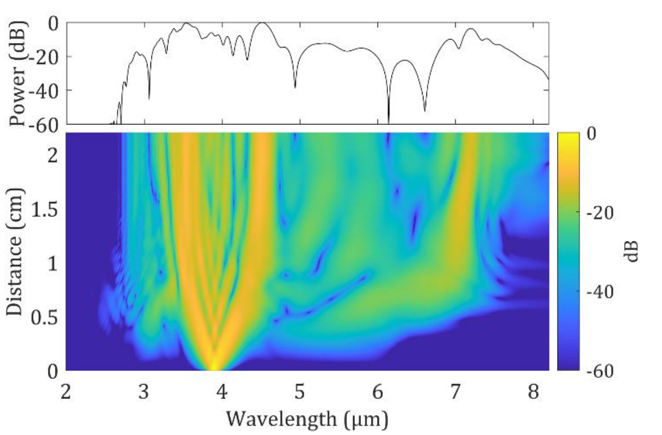

Fig. 7. Spectral evolution simulated in the 2.3 cm long tapered waveguide without the first stage narrow straight section at the input for 2.75 kW coupled peak power. Bottom: spectral evolution at different distances along the tapered waveguide, and corresponding wavelength shift of the dispersive waves. Top: Spectrum at the output of the waveguide.

V. MULTI-SPECIES GAS SPECTROSCOPY

We have seen that dips are clearly visible in the experimental spectra and we attribute these to water vapor and CO_2 absorption in the free-space path between the waveguide output and the OSA. Fig. 8a shows the SC measured out of the two-stage dispersion varying waveguide for 2.73 kW coupled peak power. The shaded cyan and gray areas highlight the spectral bandwidths where water and CO_2 strongly absorb. The former exactly corresponds to the band that was filled and flattened thanks to the particular design of our waveguide. The absorption lines observed in the spectrum correspond to the symmetric and asymmetric stretching of H_2O and the bending of CO_2 molecules. The fine structure of the absorption lines is given by the coupling of vibrational and rotational transitions [41]. Fig. 8b and 8c show the absorbance of water and CO_2 (respectively) in the spectral bands highlighted in fig. 8a, as retrieved from the measured spectrum (in blue) and from the HITRAN database (red) [42]. We can notice that, in the case of CO_2, we obtain the double branch absorption spectrum typical of roto-vibrational modes in linear molecules [41]. In the case of water, which is not a linear molecule, the absorption lines have a more complex pattern. The absorbance A is defined as:

$$A = log_{10}(\frac{I_0}{I})$$

where I_0 is the initial intensity (at the output of the waveguide) and I is the intensity of the recorded spectrum after a 55 cm long path in free space. To calculate I_0, we numerically smoothed the recorded spectrum by calculating the first order derivative, and removing the points with magnitude greater than 0.01. The absorbance from the HITRAN database was calculated multiplying the line-by-line intensity data, which give the absorption intensity for a single molecule per unit volume, by the number of molecules per unit volume and the interaction volume (air path length times beam area). By considering a concentration (in percentage by volume) of 2.7% for water vapor and 0.18% for carbon dioxide we obtain a good match between the absorbance retrieved from experiments and HITRAN (fig. 8 b, c). These values are slightly higher than what we would expect in a non-ventilated environment, meaning that our measurements might slightly overestimate the concentration of the two gases. In the case of CO_2, the absorption lines appear broader than those from HITRAN, due to the limited resolution of our OSA. The quality of these measurements could be easily improved using a gas cell, which would allow us to record a reference signal.

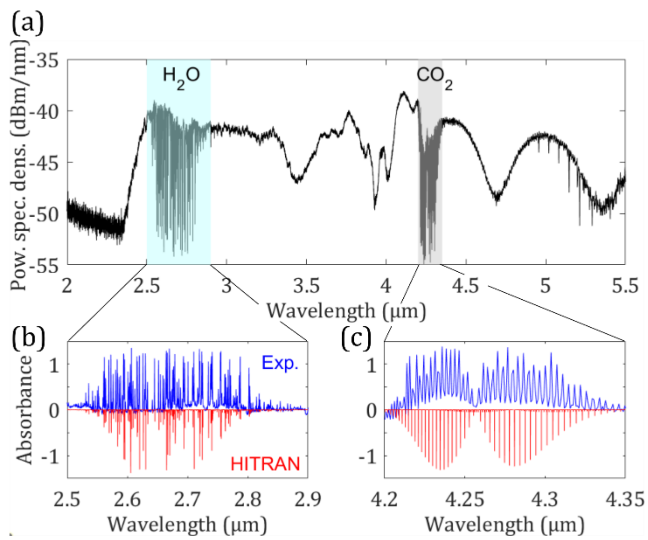

Fig. 8. (a) Power spectral density measured at the output of the two-stage dispersion varying waveguide for 2.73 kW coupled peak power. The cyan and gray shaded areas highlight the spectral bandwidths where H_2O and CO_2 strongly absorb. (b) Blue: absorbance of water retrieved from the absorption deeps in the measured spectrum. Red: absorbance calculated from data taken from HITRAN database. (c) Same as (b) for CO_2.

VI. CONCLUSION

We experimentally demonstrated efficient MIR SC generation in a SiGe/Si two-stage dispersion varying waveguide. Our particular design combines a short and narrow section waveguide with an inverse-tapered section. This allows us to improve both the efficiency of SC generation, while the continuous spectral shift of the DWs led to the generation of a flatter SC extending from 2.4 to 7.8 µm. Due to the current limitations of our experimental setup, the long wavelength extension limit was predicted by numerical simulations. The simulated SC was, at shorter wavelengths, in good agreement with experimental results, while our combined experiments and simulations clearly demonstrated the added value of our two-stage design against more commonly used straight waveguides. The enhanced bandwidth and spectral flatness of our MIR SC is of special interest for spectroscopic applications. As a proof-of-principle demonstration, we performed free-space multi-species spectroscopy of water vapor and CO_2 in the atmosphere. These measurements, which were in good agreement with reference absorption spectra from the high-resolution spectroscopy database HITRAN, enabled us to simultaneously estimate the concentration of both molecular species in the laboratory environment. Our results show the potential of efficient SC generation in dispersion managed waveguides for multi-species gas spectroscopy.

REFERENCES

[1] A. Lambrecht and K. Schmitt, *Mid-infrared gas-sensing systems and applications*. Elsevier Ltd., 2020.

[2] R. Soref, "Mid-infrared photonics in silicon and germanium," *Nat. Photonics*, vol. 4, no. 8, pp. 495–497, 2010.

[3] M. Rutkauskas, M. Asenov, S. Ramamoorthy, and D. T. Reid, "Autonomous multi-species environmental gas sensing using drone-based Fourier-transform infrared spectroscopy," *Opt. Express*, vol. 27, no. 7, p. 9578, 2019.

[4] K. H. Kim, S. A. Jahan, and E. Kabir, "A review of breath analysis for diagnosis of human health," *TrAC - Trends Anal. Chem.*, vol. 33, pp. 1–8, 2012.

[5] R. H. Wilson and H. S. Tapp, "Mid-infrared spectroscopy for food analysis: Recent new applications and relevant developments in sample presentation methods," *TrAC - Trends Anal. Chem.*, vol. 18, no. 2, pp. 85–93, 1999.

[6] D. Popa and F. Udrea, "Towards integrated mid-infrared gas sensors," *Sensors*, vol. 19, no. 9, pp. 1–15, 2019.

[7] H. Lin *et al.*, "Mid-infrared integrated photonics on silicon: A perspective," *Nanophotonics*, vol. 7, no. 2, pp. 393–420, 2017.

[8] D. Marris-Morini *et al.*, "Germanium-based integrated photonics from near- to mid-infrared applications," *Nanophotonics*, vol. 7, no. 11, pp. 1781–1793, 2018.

[9] V. Reboud *et al.*, "Germanium based photonic components toward a full silicon/germanium photonic platform," *Prog. Cryst. Growth Charact. Mater.*, vol. 63, no. 2, pp. 1–24, 2017.

[10] G. Z. Mashanovich *et al.*, "Group IV mid-infrared photonics [Invited]," *Opt. Mater. Express*, vol. 8, no. 8, pp. 1040–1043, 2018.

[11] F. Kapsalidis *et al.*, "Dual-wavelength DFB quantum cascade lasers: sources for multi-species trace gas spectroscopy," *Appl. Phys. B Lasers Opt.*, vol. 124, no. 6, pp. 1–17, 2018.

[12] L. A. Sterczewski *et al.*, "Mid-infrared dual-comb spectroscopy with interband cascade lasers," *Opt. Lett.*, vol. 44, no. 8, p. 2113, 2019.

[13] J. Rouxel *et al.*, "Miniaturized differential Helmholtz resonators for photoacoustic trace gas detection," *Sensors Actuators, B Chem.*, vol. 236, pp. 1104–1110, 2016.

[14] A. L. Gaeta, M. Lipson, and T. J. Kippenberg, "Photonic-chip-based frequency combs," *Nat. Photonics*, vol. 13, no. 3, pp. 158–169, 2019.

[15] E. Tagkoudi, D. Grassani, F. Yang, C. Herkommer, T. J. Kippenberg, and C.-S. Brès, "Parallel gas spectroscopy using mid-infrared supercontinuum from a single Si3N4 waveguide," *Opt. Lett.*, vol. 45, no. April, pp. 2195–2198, 2020.

[16] R. K. W. Lau, M. R. E. Lamont, A. G. Griffith, Y. Okawachi, M. Lipson, and A. L. Gaeta, "Octave-spanning mid-infrared supercontinuum generation in silicon nanowaveguides.," *Opt. Lett.*, vol. 39, no. 15, pp. 4518–21, 2014.

[17] N. Singh *et al.*, "Midinfrared supercontinuum generation from 2 to 6 µm in a silicon nanowire," *Optica*, vol. 2, no. 9, p. 797, 2015.

[18] N. Nader *et al.*, "Infrared frequency comb generation and spectroscopy with suspended silicon nanophotonic waveguides," *Optica*, vol. 6, no. 10, pp. 1269–1276, 2019.

[19] M. Sinobad *et al.*, "Mid-infrared octave spanning supercontinuum generation to 8.5 µm in silicon-germanium waveguides," *Optica*, vol. 5, no. 4, p. 360, 2018.

[20] M. Sinobad *et al.*, "Dispersion trimming for mid-infrared supercontinuum generation in a hybrid chalcogenide/silicon-germanium waveguide," *J. Opt. Soc. Am. B*, vol. 36, no. 2, pp. A98--A104, 2019.

[21] M. Sinobad *et al.*, "High coherence at f and 2f of mid-infrared supercontinuum generation in silicon germanium waveguides," *IEEE J. Sel. Top. Quantum Electron.*, vol. 26, no. 2, pp. 1–8, 2020.

[22] M. Sinobad *et al.*, "Mid-infrared supercontinuum generation in silicon-germanium all-normal dispersion waveguides," *Opt. Lett.*, vol. 45, no. 18, pp. 5008–5011, 2020.

[23] M. Montesinos-Ballester *et al.*, "On-Chip Mid-Infrared Supercontinuum Generation from 3 to 13 µm Wavelength," *ACS Photonics*, vol. 7, no. 12, pp. 3423–3429, 2020.

[24] A. Della Torre *et al.*, "Mid-infrared supercontinuum generation in a low-loss germanium-on-silicon waveguide Mid-infrared supercontinuum generation in a low-loss germanium-on-silicon waveguide," *APL Photonics*, vol. 6, no. 1, p. 016102, 2021.

[25] J. M. Dudley, G. Genty, and S. Coen, "Supercontinuum generation in photonic crystal fiber," *Rev. Mod. Phys.*, vol. 78, no. 4, pp. 1135–1184, 2006.

[26] A. M. Heidt *et al.*, "Coherent octave spanning near-infrared and visible supercontinuum generation in all-normal dispersion photonic crystal fibers," *Opt. Express*, vol. 19, no. 4, p. 3775, 2011.

[27] J. W. Lou, T. J. Xia, O. Boyraz, C. X. Shi, G. A. Nowak, and M. N. Islam, "Broader and flatter supercontinuum spectra in dispersion-tailored fibers," in *Proceedings of Optical Fiber Communication Conference*, 1997, pp. 32–34.

[28] K. Mori, H. Takara, S. Kavanishi, M. Saruwatari, and T. Morioka,

"Flatly broadened supercontinuum spectrum generated," *Electron. Lett.*, vol. 33, no. 21, pp. 1806–1808, 1997.

[29] T. A. Birks, W. J. Wadsworth, and P. S. J. Russell, "Supercontinuum generation in tapered fibres," *Opt. Lett.*, vol. 25, no. 19, pp. 1415–1417, 2000.

[30] J. Teipel *et al.*, "Characteristics of supercontinuum generation in tapered fibers using femtosecond laser pulses," *Appl. Phys. B Lasers Opt.*, vol. 77, no. 2–3, pp. 245–251, 2003.

[31] F. Lu and W. H. Knox, "Generation of a broadband continuum with high spectral coherence in tapered single-mode optical fibers," *Opt. Express*, vol. 12, no. 2, p. 347, 2004.

[32] F. Lu, Y. Deng, and W. H. Knox, "Generation of broadband femtosecond visible pulses in dispersion-micromanaged holey fibers," *Opt. Lett.*, vol. 30, no. 12, p. 1566, 2005.

[33] J. Teipel, D. Turke, H. Giessen, A. Zintl, and B. Braun, "Compact multi-Watt picosecond coherent white light sources using multiple-taper fibers," *Opt. Express*, vol. 13, no. 5, p. 1734, 2005.

[34] G. Humbert *et al.*, "Supercontinuum generation system for optical coherence tomography based on tapered photonic crystal fibre," *Opt. Express*, vol. 14, no. 4, p. 1596, 2006.

[35] A. Kudlinski *et al.*, "Zero-dispersion wavelength decreasing photonic crystal fibers for ultraviolet-extended supercontinuum generation," *Opt. Express*, vol. 14, no. 12, p. 5715, 2006.

[36] Z. Chen, A. J. Taylor, and A. Efimov, "Coherent mid-infrared broadband generation in non-uniform ZBLAN fiber taper," *Opt. Express*, vol. 17, no. 7, pp. 5852–5860, 2009.

[37] N. Singh *et al.*, "Supercontinuum generation in varying-dispersion and birefringent silicon waveguide," *Opt. Express*, vol. 27, no. 22, pp. 31698–31712, 2019.

[38] J. Wei, C. Ciret, M. Billet, F. Leo, B. Kuyken, and S. P. Gorza, "Supercontinuum Generation Assisted by Wave Trapping in Dispersion-Managed Integrated Silicon Waveguides," *Phys. Rev. Appl.*, vol. 14, no. 5, p. 054045, 2020.

[39] J. Leuthold, C. Koos, and W. Freude, "Nonlinear silicon photonics," *Nat. Photonics*, vol. 4, no. 8, pp. 535–544, 2010.

[40] M. R. Karim, N. Al Kayed, N. Jahan, M. S. Alam, and B. M. A. Rahman, "Study of Highly Coherent Mid-Infrared Supercontinuum Generation in CMOS Compatible Si-rich SiN Tapered Waveguide," *J. Light. Technol.*, vol. 8724, pp. 1–12, 2022.

[41] J. M. Hollas, *Modern Spectroscopy*. John Wiley & Sons, 2004.

[42] L. S. Rothman *et al.*, "The HITRAN 2012 Molecular Spectroscopic Database," *J. Quant. Spectrosc. Ra., Elsevier, ISSN*, vol. 130, pp. 4–50, 2013.

Alberto Della Torre received the B.Sc. degree in engineering physics from the Polytechnic of Milan, Italy, in 2015, the M.Sc. degree in nanoscale engineering and Ph.D in integrated photonics from the Ecole Centrale de Lyon, France, in 2017 and 2021, respectively. Currently, he is a postdoctoral researcher at the Institut des Nanotechnologies de Lyon, Ecole Centrale de Lyon, France. His research interests include integrated photonics, nonlinear optics, and mid-infrared photonics.

Rémi Armand received the B.S. degree in electrical engineering from the Ecole Normal Supérieur de Cachan, Cachan, France, in 2015, and the M.S. degree in electrical engineering from the Université Paris-Saclay, Saclay, France, in 2018. He is currently working toward the Ph.D. degree in physics with the Ecole Centrale de Lyon, Ecully, France. His research interests include the design of structure to generate mid-infrared broadbrand sources, and fundamental study of nonlinear photonics.

Milan Sinobad is a postdoctoral associate researcher working on integrated femtosecond lasers at the Ultrafast Optics and X-Rays group at the Center for Free-Electron Laser Science at DESY. He received his Dipl. Ing. degree from the University of Belgrade, M. Sci. degree from University of Lyon, and a Ph.D. degree from the Royal Melbourne Institute of Technology in 2020. His research interests include nonlinear and ultrafast optics, silicon photonics, and laser physics.

Kokou Firmin Fiaboe received the B.S. degree in electrical engineering from the Ecole Nationale Supérieure d'Ingénieurs (Université de Lomé), Lome, Togo, in 2016, and M. Tech. degree in electronic and telecommunication engineering from Kalinga Institut of Industrial Technology, Bhubaneswar, India, in 2019. He is currently working toward the Ph.D. degree in integrated photonics with both Ecole Centrale de Lyon, Ecully, France and Royal Melbourne Institute of Technology, Melbourne, Australia. His research interests include the design and fabrication of on-chip mid-infrared broadbrand sources, and nonlinear photonics.

Barry Luther Davies received the B.Sc. and Ph.D. degrees in laser physics and nonlinear optics from the University of Southampton, Southampton, U.K. He is currently an Emeritus Professor in the Department of Quantum Science and Technology at the Australian National University (ANU), Canberra, Australia, with experience in the diverse areas of research including lasers, laser–matter interaction physics, photonics, optical materials, and nonlinear optics. He joined the ANU in 1974, where he led a team working on the physics of laser-produced plasmas, until the early 1990s, when the research evolved into studies of laser-materials processing and pulsed laser deposition of thin films. More recently, he has specialized in nonlinear optical materials and devices and photonics with a strong interest in the development of devices for optical signal processing and for mid-infrared science. He has published more than 400 papers and book chapters. Professor Luther-Davies is a Fellow of the Optical Society of America and the Australian Academy for Technological Sciences and Engineering. He was awarded the Pawsey Medal of the Australian Academy of Science and the Beattie Steel Medal of the Australian and New Zealand Optical Society.

Stephen J. Madden received the B.Sc. degree in electronic engineering and the Ph.D degree in integrated optics from Imperial College in London, London, U.K., in 1985 and 1989, respectively. He is Associate Professor and a Fellow with Laser Physics Centre, Australian National University (ANU), Canberra, Australia. He has spent most of his career in industry. In 1991, he joined the Telstra Research Laboratories, Melbourne, Australia. In 1997, he became the Director of Research at ADC Telecommunications, Minneapolis, MN, USA, before leaving to become VP engineer with the Sparkolor Corporation, Santa Clara, CA, USA, in 2001. More recently, he led a research within CUDOS, a research consortium between seven Australian universities, into photonics devices. He has published more than 200 papers.

Arnan Mitchell received the Ph.D. degree in engineering from RMIT University, Melbourne VIC, Australia, in 2000. He is a Distinguished Professor with the School of Engineering, RMIT University, Bundoora, Australia, and is Director of RMIT Micro Nano Research Facility. He is a highly multidisciplinary researcher working in microchip technologies combining light, sound, fluids, and electronics with applications spanning radar systems for defense, high-speed fiber-optic communications, and point-of-care diagnostic systems for biomedicine. He is enthusiastic about translating technology into the hands of end-users and has dedicated much of his career to building diverse teams and comprehensive micro and nanotechnology infrastructure to enable breakthrough discoveries to achieve real-world impact.

Thach Nguyen is a Senior Lecturer in the Electronics & Telecommunications Discipline - School of Engineering and was an ARC APD fellow. He completed his PhD at RMIT University on highly efficient LiNbO3 modulators. His current research interests include integrated photonic devices and circuits, integrated photonic design methods, numerical methods for integrated photonics, and microwave photonics. He has created a number of integrated photonic design and simulation tools.

David J. Moss ((S'83–M'88–SM'09–F'16) received the B.Sc. degree in physics from the University of Waterloo, Waterloo, ON, Canada, and the M.Sc. and Ph.D. degrees in nonlinear optics from the University of Toronto, Toronto, ON, in 1983 and 1988, respectively. He is the Director of the Optical Sciences Centre at Swinburne University of Technology, Melbourne, Australia, leading research programs in integrated nonlinear nanophotonics, microwave photonics, telecommunications, quantum optics, biophotonics, renewable energy, and other areas. From 1988 to 1992, he was with the National Research Council of Canada, Institute for Microstructural Sciences, Ottawa, Canada, working on III–V optoelectronic devices. From 1992 to 1994, he was a Senior Visiting Scientist with the Hitachi Central Research Laboratories, Tokyo, Japan, working on high-speed optoelectronic devices for 10-Gb/s fiber-optic telecommunications systems. From 1994 to 1998, he was a Senior Research Fellow with the Optical Fiber Technology Centre, University of Sydney, Australia. From 1998 to 2003, he was a Manager with JDS Uniphase, Ottawa, Canada, leading a team developing products for 40-Gb/s telecommunications systems. From 2003 to 2013, he was with the University of Sydney and the Centre for Ultra-High Bandwidth Devices for Optical Systems working on ultrahigh bandwidth optical signal processing, integrated nonlinear nanophotonic circuits, and photonic crystal devices. Prof. Moss received the 2011 Australian Museum Eureka Science Prize and the Google Australia Award for innovation in computer science. He is a Fellow of the IEEE Photonics Society, a Fellow of Optica, and the SPIE

Jean-Michel Hartmann received the Ph.D. degree in physics from Université Grenoble Alpes, France, in 1997. He joined CEA, Leti, Grenoble, France, in 1999, as a SiGeC Epitaxy Research Scientist. He was a Postdoctoral Fellow with the Imperial College, London, U.K. He is currently coordinating group-IV epitaxy activities in Leti's Technological PlatForm Department. He has the rank of CEA Research Director.

Vincent Reboud received his PhD in Physics in 2004 from the University of Paris-Sud, Orsay, France. He joined after the Tyndall National Institute in Ireland to work on optical components realized in nanoimprinted functionalized materials. He followed up his research in the Catalan Institute of Nanotechnology in Spain to study reconfigurable optical surfaces and 3D hybrid surfaces and worked then on optoelectronic components patterned by wafer-scale nanoimprint lithography in CEA-LETI, France. In 2014, he joined the Silicon Photonics and the Optical Sensing Lab of CEA-LETI as a senior scientist to work on group-IV light sources and detectors for optical sensors and on IR & MIR photonics platform for a broad range of applications.

Jean-Marc Fédéli received the Electronics Engineer Diploma from INPG Grenoble, Grenoble, France, in 1978. He was involved in the development of various magnetic memories and magnetic components as Project Leader, Group Leader, and Program Manager with the CEA-LETI, Grenoble, France. For two years, he was Advanced Program Director with the Memscap Company, France, for the development of RF-MEMS, then with the CEA-LETI in 2002 as a Coordinator of silicon photonic projects until 2012. Under a larger research partnership, he works on many technological aspects on photonics on CMOS (Si rib and stripe waveguides, a-Si waveguides, slot waveguides), Si modulators, Ge photodetectors, and InP integrated sources on Si. He has been participating in different European projects such as EPIXFAB for MPW circuit fabrication and has coordinated the FP7 PLAT4M project on Silicon Photonics Platform. In 2014, he has moved to sensing activities with photonics, and he was the Technical Manager of the H2020 MIRPHAB pilot line on liquid and gas systems sensors. His H factor is around 35 with more than 200 publications and 50 patents. He is the author of three book chapters (one on magnetic recording and two on silicon photonics). He is now retired.

Christelle Monat (M'08) received the Ph.D. degree in electronic integrated devices from the Ecole Centrale de Lyon, Ecully, France, in 2003. She was with the École Polytechnique Fédérale de Lausanne, Switzerland, for two years, where she was involved in research on single-photon sources. She joined the Centre for Ultrahigh-bandwidth Devices for Optical Systems (CUDOS), School of Physics, University of Sydney, Australia, in late 2005 and led the research on slow light-enhanced nonlinear optics between 2007 and 2010. From 2010 to 2019, she has been an Associate Professor with the Institut des Nanotechnologies de Lyon, Ecole Centrale de Lyon, and was awarded an ERC consolidator grant on graphene-based nonlinear photonic integrated circuits in 2015. Since 2019, she is Full Professor at the Institut des Nanotechnologies de Lyon, Ecole Centrale de Lyon. Her current research interests include

This article has been accepted for publication in IEEE Journal of Selected Topics in Quantum Electronics. This is the author's version which has not been fully edited and content may change prior to final publication. Citation information: DOI 10.1109/JSTQE.2022.3185169

slow light, photonic crystals, III–V Si hybrid photonics, microlasers, and nonlinear optics in the near- and mid-IR.

Christian Grillet received the Ph.D. degree in electronic integrated devices from the Ecole Centrale de Lyon, Ecully, France, in 2003. In 2004, he joined the Centre for Ultrahigh-bandwidth Devices for Optical Systems (CUDOS), University of Sydney, Sydney, Australia. He then joined Centre national de la recherche scientifique (CNRS), Paris, France, in 2013. He leads the International Associated Laboratory in Photonics between France and Australia (LIA ALPhFA). His research interests include integrated nonlinear optics, mid-infrared integrated optics, photonic crystals, and slow light.